

Multi-Objective Optimization of Turbofan Design Parameters for an Advanced, Single-Aisle Transport

Jeffrey J. Berton*

NASA Glenn Research Center, Cleveland, Ohio 44135

and

Mark D. Guynn†

NASA Langley Research Center, Hampton, Virginia 23681

Considerable interest surrounds the design of the next generation of single-aisle commercial transports in the Boeing 737 and Airbus A320 class. Aircraft designers will depend on advanced, next-generation turbofan engines to power these airplanes. The focus of this study is to apply single- and multi-objective optimization algorithms to the conceptual design of ultrahigh bypass (UHB) turbofan engines for this class of aircraft, using NASA's Subsonic Fixed Wing Project goals as multidisciplinary objectives for optimization. The independent propulsion design parameters investigated are aerodynamic design point fan pressure ratio, overall pressure ratio, fan drive system architecture (i.e., direct- or gear-driven), bypass nozzle architecture (i.e., fixed- or variable-geometry), and the high- and low-pressure compressor work split. NASA Project goal metrics – fuel burn, noise, and emissions – are among the parameters treated as dependent objective functions. These optimized solutions provide insight to the UHB engine design process and provide independent information to NASA program management to help guide its technology development efforts. This assessment leverages results from earlier NASA system concept studies conducted in 2008 and 2009, in which UHB turbofans were examined for a notional, next-generation, single-aisle transport. The purpose of these NASA UHB engine concept studies is to determine if the fuel consumption and noise benefits of engines having lower fan pressure ratios (and correspondingly higher bypass ratios) translate into overall aircraft system-level benefits for a 737 class vehicle.

Nomenclature

ADP	= aerodynamic design point
AFE	= above field elevation
$ANOPP$	= Aircraft Noise Prediction Program
D_L	= landing field length
D_{TO}	= takeoff field length
$EPNL$	= effective perceived noise level
f_i	= optimization objective functions
$FLOPS$	= Flight Optimization System
$F_{N,mapp}$	= missed approach excess net thrust
$F_{N,SLS}$	= sea level static thrust
$F_{N,ss}$	= second segment climb excess net thrust
FPR	= fan pressure ratio
g_i	= optimization inequality design constraints
$\dot{h}_{pot,toc}$	= potential rate of climb at top of climb conditions
ISA	= international standard atmosphere

* Aerospace Engineer, Multidisciplinary Design, Analysis and Optimization Branch, MS 5-11, senior member AIAA

† Aerospace Engineer, Aeronautics Systems Analysis Branch, MS 442, senior member AIAA

<i>LTO</i>	=	landing and takeoff operational cycle for emissions regulations
<i>NM_{Cum}</i>	=	cumulative noise margin relative to the stage 4/chapter 4 rule
<i>NO_x</i>	=	oxides of nitrogen (nitric oxide and nitrogen dioxide) exhaust emissions
<i>NPSS</i>	=	Numerical Propulsion System Simulation
<i>NSGA-II</i>	=	Non-dominated, Sorting Genetic Algorithm (version II)
<i>OPR</i>	=	engine overall pressure ratio
<i>PDCYL</i>	=	Point Design of Cylindrical-bodied Aircraft
<i>PR</i>	=	pressure ratio
<i>SLS</i>	=	sea level static
<i>S_w</i>	=	reference trapezoidal wing area
<i>x_i</i>	=	optimization design parameters
<i>UHB</i>	=	ultrahigh bypass
<i>v_{app}</i>	=	approach velocity
<i>WATE</i>	=	Weight Analysis of Turbine Engines
<i>W_{block fuel}</i>	=	block fuel weight
<i>W_{excess fuel}</i>	=	excess fuel weight
<i>W_{ramp}</i>	=	ramp weight

I. Introduction

NASA sets aggressive, strategic, civil aircraft performance and environmental goals and develops ambitious technology roadmaps to guide its technology research efforts. Under NASA's Fundamental Aeronautics Program, the Subsonic Fixed Wing Project has adopted fuel efficiency, community noise, exhaust emissions, and takeoff field length goals for the new, subsonic, single-aisle, civil aircraft expected to replace the current Boeing 737 and Airbus A320 families of airplanes. Relative to B737-800/CFM56-7B performance levels, NASA goals call for 33% reductions in block fuel burn and takeoff field length. The NASA goal for oxides of nitrogen (NO_x) is 60% below the landing and takeoff emission stringencies set in 2004 by the Committee on Aviation Environmental Protection (CAEP/6). Additionally, these aircraft are to achieve certification noise levels 32 cumulative EPNdB under current FAA Stage 4/ICAO Chapter 4 noise limits.

Since these performance metrics are aggressive, contrasting, and often conflicting, achieving goal levels for the fuel burn, noise, emissions, and field length metrics simultaneously may not be possible. These goals therefore may represent distinct "corners" of the airplane design trade space. A balanced, profitable, business-case airplane design may satisfy one or more of these goals, but is unlikely to meet the goal of every metric at once.

The multidisciplinary design and analysis of an advanced, single-aisle civil airplane lends itself well to single- and multi-objective optimization. In this study, the NASA goals for performance, noise, and emissions serve as the basis for this practical optimization problem with important implications for the product's design and expectations.

This assessment leverages tools, methods, and results from earlier NASA system concept studies conducted in 2008 and 2009, in which ultrahigh bypass (UHB) turbofan engines were examined for a notional, single-aisle transport.^{1, 2, 3} A parallel acoustics study of the airplane was also performed.⁴ The objective of the NASA UHB engine concept studies was to determine if the fuel consumption and noise benefits of engines having lower fan pressure ratios (and correspondingly higher bypass ratios) translate into overall aircraft system-level benefits for a 737 class vehicle. Such independent information is important to help NASA program management guide its own technology development efforts.

In Refs. 1-3, the propulsion system conceptual design trade space was examined by designing a representative family of 48 UHB engines, analytically installing them on a common airframe model, and performing aircraft mission performance and sizing analyses. The independent propulsion design parameters investigated were aerodynamic design point fan pressure ratio, overall pressure ratio, fan drive system architecture (i.e., direct- or gear-driven), bypass nozzle architecture (i.e., fixed- or variable-geometry), high- and low-pressure compressor compression work split, and cruise Mach number.

In this study, all of the above design parameters (except for the design cruise Mach number) are treated as independent mathematical parameters subject to optimization. Aircraft performance characteristics, including properties of the NASA project goal metrics (fuel burn, emissions, and noise), as well as ramp weight, are analytically computed and are treated as dependent mathematical objective functions.

Significant fuel and cost reductions are necessary to justify the development of a new, single-aisle transport, or to justify retrofitting current aircraft with new engines. Noise and exhaust emissions reduction will continue to be of increasing importance as the demand for air travel grows. Substantial reductions in noise and emissions are required

to enable unconstrained aviation growth without negatively impacting the environment. The expectation of this analysis is to broaden the solutions obtained during the studies of Refs. 1-3 with the additional objectives of fuel, noise, and exhaust emissions included as subjects of optimization. This single- and multi-objective optimization provides insight to the engine design options that will be necessary to achieve multiple goals.

II. Method of Analysis

Once expected to enter service as early as 2015, it now appears a 737 replacement aircraft will be delayed for several more years.⁵ And as of this writing, Boeing may yet proceed with a 737 engine retrofit program rather than proceed with a new, “clean sheet” airplane design.⁶ Nonetheless, a notional airplane intended to represent an all-new, 737 replacement equipped with new UHB turbofans is modeled here. Engine component and subsystem performance, hot section cooling levels, and material technologies appropriate for an approximate 2015-2020 service entry date are assumed. Airframe technologies commensurate with a 2015-2020 service entry date are also assumed.

The tools and procedures described in Ref. 1 have essentially been automated so that the entire multidisciplinary analysis may be driven by a multi-objective optimizer. This is no small feat, as many heuristic design rules are necessarily added in order to remove the engineer from the loop without introducing errors. Each disciplinary analysis is summarized below.

A. Propulsion System

The basic engine architecture is a boosted, two-spool, separate-flow turbofan.* The propulsion system independent design parameters subject to optimization are the fan pressure ratio (FPR) at the aerodynamic design point (ADP), the overall pressure ratio (OPR) at the ADP, the fan drive system architecture (i.e., direct- or gear-driven), the bypass nozzle architecture (i.e., fixed- or variable-geometry), and the high- and low-pressure compressor compression work split.

A multiple design point analysis is performed on the engine cycle in order to meet several performance requirements such as airplane thrust demand at rolling takeoff and top-of-climb conditions, as well as to set flow rates, cycle temperatures, pressures, spool speeds, and cooling levels. The cycle ADP is at the top-of-climb condition (Mach 0.80, 35kft, ISA+0), and the rolling takeoff condition is at sea level, Mach 0.25, ISA+27°F. Turbomachinery is represented by scaled component performance maps. Additional details on the engine design, material selections, and engine technology level assumptions may be found in Refs. 1-3.

The thermodynamic engine cycle performance is analyzed using the Numerical Propulsion System Simulation code (NPSS^{7, 8}). NPSS is a variable-fidelity, object-oriented, engine cycle analysis tool developed jointly by NASA and U.S. industry. It is currently the accepted, state-of-the-art software for airbreathing engine cycle performance analysis for U.S. aerospace industry, academia, and NASA. Aeromechanical design, flowpath, and engine weight analyses are performed with the Weight Analysis of Turbine Engines code (WATE⁹). WATE has been significantly upgraded since its initial introduction in the 1970s and is currently implemented as a suite of NPSS interpretive analysis elements. At NASA, WATE is coupled with NPSS to provide a complete modeling capability of turbofan engines.

The design FPR has a large influence over an engine’s performance, dimensions, and weight. Its value, along with the ratio of pressure levels in the bypass and core exhaust ducts (the extraction ratio), sets the bypass ratio – a major determinant of an engine’s fuel consumption characteristics. Bypass ratio is inversely proportional to FPR; as FPR is reduced, fan airflow must increase in order to maintain thrust requirements. Constant design fan loading is assumed in this analysis, therefore the choice of FPR sets the fan tip speed and the rotation rate of the low-pressure spool. FPR is also a major consideration in setting the design airflow, and thus it factors into the overall diameter, weight, wetted area, and drag of the propulsion system. The choice of FPR also has a considerable effect on the low-pressure turbine design, particularly in cases where no fan gearbox is present. It is selected for optimization as a continuously-variable, real, independent parameter. The range of values considered is 1.35 to 1.70; the approximate practical limits for large, single-stage fans.

The design OPR also has a large influence over cycle performance, with higher OPRs providing the benefits of higher engine thermal efficiencies. It also has implications in exhaust NO_x emissions, as discussed below. Treating OPR as another continuously-real design parameter, however, leads to excessive computational time. Instead, it is treated here as a binary-logical design switch, with ADP values of 42 representing a “high” setting, and 32 a “low”

*Three-spool engines represent another potentially viable turbofan architecture for this aircraft class, but they are not investigated here.

setting. An ADP OPR of 42 is the approximate upper limit for this type and class of engine. With reasonable compressor disk and compressor exit Mach number design assumptions, an OPR of 42 leads to compressor annular exit passage heights of approximately one-half inch (a typical limiting constraint used in axial turbomachinery design).

An engine design parameter related to OPR is the compression work split between the high- and low-pressure compressors. For a given fan pressure ratio and overall pressure ratio, the “low work” engines have a lower pressure rise across the low-pressure compressor (and a correspondingly higher pressure rise across the high pressure compressor) compared to the “high work” engines. For example, in engines having an ADP OPR of 42, the high-pressure compressor pressure ratio is 17.7 for the “low work” designs, but it is only 12.0 for the “high work” designs. The low-pressure compressor pressure ratio is selected to produce the desired OPR as FPR varies. The compression work split design parameter is also represented by a binary-logical switch, rather than by a continuously-real parameter. More information on how the work split logic is implemented may be found in Refs. 1-3.

Low FPR engine cycles generally require some type of variable geometry for proper operation throughout the flight envelope. Without variable geometry, a sufficiently low ADP FPR at altitude will lead to a fan surge problem when operating near sea level. The most attractive way to solve this problem may be with a variable-geometry bypass nozzle. The nozzle exit opens when operating near sea level, and the resulting increase in flow area shifts the fan operating point away from the surge line. The variable-geometry nozzles in the analysis are assessed a 10% weight penalty relative to equivalent fixed-geometry designs. The exit areas of the variable nozzles are varied at off-design using an NPSS solver balance to maintain a constant fan operating line. Engines equipped with variable-geometry nozzles therefore enjoy operation near peak fan efficiencies, albeit at the cost of added nozzle weight. Whenever the optimizer naively “creates” an engine by coupling a fixed-geometry nozzle with a low-pressure fan, the fan design surge margin is automatically increased so that the fan always operates with an adequate surge margin in off-design conditions. This results in the fan operating at very low fan efficiencies during cruise. Of course, in reality, a low-pressure fan would never be designed with a fixed-geometry nozzle, but it is possible in the analytical world. The punishing effects of a very high design fan surge margin should naturally cause the optimizer to avoid these designs.

The choice of the fan drive system architecture is a major propulsion design consideration. At reasonable fan loadings, a fan having a low design pressure ratio spins relatively slowly. Without a gearbox, the low-pressure turbine (LPT) must rotate at the same low speed. This sets up the classical shaft speed mismatch for two-spool turbofans having low design fan pressure ratios. The LPT diameter cannot simply be increased to maintain high, efficient tip speeds without weight penalties and without obstructing the flow in the bypass duct. The stage count of the LPT in a conventionally-driven turbofan therefore must increase as the design FPR is reduced if reasonable LPT loadings are maintained, which adds considerable weight and length to the engine. Exacerbating the problem is the high gas temperatures in the hot section of the engine (relative to those in the fan), which effectively elevates the speed of sound and lowers the tip Mach numbers of the LPT. The shaft speed mismatch can be altogether avoided by using a gearbox, which enables the fan and the low-pressure spool to operate at different rotational speeds. Use of a gear system does, however, introduce a separate set of concerns such as gearbox weight, reliability, and cost. In this study, a binary-logical design switch determines if a fan gearbox is present. The optimizer will frequently (and naively) design an engine with a directly-driven fan having a low FPR. Such poorly-designed systems will have a large number of LPT stages (and low-pressure compressor stages, particularly in the case of our “high work” engines). But, like the situation discussed above with the variable-geometry bypass nozzle design switch, the resulting poor objective values should steer the optimizer away from these designs.

B. Airplane

It is not sufficient to determine aircraft benefits from engine characteristics alone. Improvements in fuel consumption, for example, often come at the expense of engine size and weight. Only by combining the engines with an airframe model can the net impact of an engine design be captured. Aircraft synthesis and sizing analyses are carried out using NASA’s Flight Optimization System (FLOPS,¹⁰ v8.0) computer program. Special sizing considerations introduced by large-diameter, UHB engines are addressed through enhancements to the FLOPS analysis. Spreadsheet analyses are used to determine landing gear length, engine-out drag, and required vertical tail size so that impacts of large-diameter engines are properly captured. Enhancements to basic FLOPS capabilities are also made in the structural weight and aerodynamics areas. The wing and fuselage structural weight estimates of FLOPS are replaced with estimates from PDCYL.¹¹ PDCYL offers a less empirical, more analytical weight estimation methodology that is more sensitive to parameters such as engine weight and location. FLOPS

aerodynamic predictions are enhanced through a model calibration process incorporating details of the 737-800 high speed and low speed aerodynamic performance.

1. Baseline Airframe Model

The notional airplane is based on an analytical evolution of the currently-in-service Boeing 737-800 with winglets. In Ref. 1, a reference 737 analytical model was developed based on publicly-available 737-800 geometry, weight, and performance information; proprietary low-speed and clean-configuration aerodynamic data; and a NASA NPSS representation of the CFM56-7B engine. The CFM56-7B was analytically modeled in NPSS using data available from several public-domain sources, such as FAA type certification data sheets, manufacturer-provided operating documents, technical reports, Jane's Aero-Engines,¹² and manufacturer's websites. No company-proprietary propulsion data were used. The reference 737 carries 162 passengers in a single-aisle, two-class seating arrangement. Minor calibrations to the FLOPS-computed component weights and aerodynamics were performed to match published operating empty weight and range capability of 3060 nm at a 32,400 lb payload. The FLOPS model was set up to perform a basic wing-engine sizing analysis. Scaling the wing and engine sizes of the reference model for minimum ramp weight subject to active aircraft performance constraints led to results that were consistent with the actual 737 aircraft.

2. Advanced Airframe Model

To transform the reference 737 into the advanced vehicle model, the design cruise Mach number is increased from 0.785 to 0.800, with an appropriate increase in wing sweep to reflect the higher airspeed. The wing aspect ratio and taper ratio are unchanged. The 162-passenger, mixed-class, single-aisle cabin arrangement is maintained, but the design range at the 32,400 lb payload point is increased from 3060 nm to 3250 nm. The performance improvements in airspeed and range are considered appropriate for a future vehicle in this class. Broad use of composite structural materials is assumed relative to the predominantly-metal construction of the 737. This is comparable to the structure of the new Boeing 787, where as much as 50 percent of the primary structure is made of composites.¹³ Composite construction of primary structures is assumed to result in a 15% reduction in the component weights computed for the wing, fuselage, and empennage. Additional technology improvements similar to those found on the 787 include an increase in hydraulic pressure to 5000 psi and a 1% reduction in drag due to trailing edge variable camber and drag clean-up. A Vehicle Sketch Pad¹⁴ planform schematic of the vehicle is shown in Fig. 1. This vehicle is the common airframe model for all of the propulsion systems analyzed.

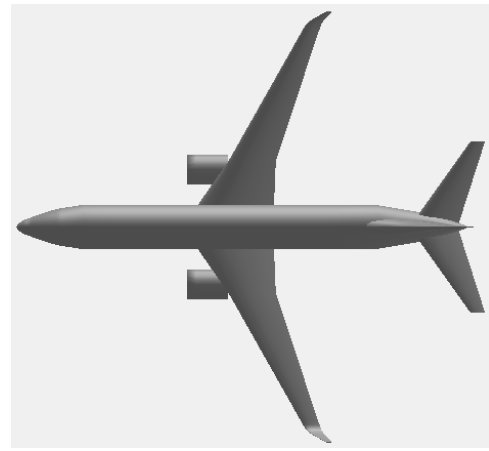


Figure 1. Planform view of the notional, advanced, single-aisle transport.

C. Takeoff and Landing Trajectory Analysis

An interesting and important aspect of the aircraft-engine system not always considered in noise certification predictions is the influence of airplane trajectory and engine throttling on noise. UHB turbofans have significantly different thrust lapse characteristics than other turbofans having higher specific thrust, resulting in takeoff and approach trajectories and throttle settings that must be modeled properly to correctly predict certification noise. Detailed takeoff and approach trajectory calculations are automatically made for every airplane and engine designed by the optimizer. These trajectory calculations are used to establish the field length of each airplane as well as for its certification noise levels.

Detailed, low-speed takeoff and landing assessments are made using FLOPS's built-in, time-stepping trajectory analysis module. Proprietary low-speed aerodynamic data for several flap and slat settings, thrust performance, and aircraft weights are inputs to the analysis. Compliance with the airworthiness requirements described in Part 25 and 36 of the Federal Aviation Regulations (Refs. 15 and 16, respectively) are observed. The low-speed trajectory analysis is validated for the baseline airframe model using performance data¹⁷ of a 737 taking off and landing under standard day, dry runway conditions. Takeoff and landing distances for the baseline airframe model match to within approximately one percent of the reported values. The same analysis is used to predict the trajectories of the advanced airframe model.

A noise abatement throttle cutback occurs in all cases between 16,000 ft and 17,000 ft from brake release. The engine climb thrust at this distance is reduced to the minimum level permitted by regulation (i.e., Ref. 16 requires a minimum climb gradient of four percent with both engines operating, or level flight with one engine inoperative.). The power cutback typically takes place at approximately 1200 ft AFE, depending on the characteristics of the engine and airplane designed by the optimizer. This is always above the minimum altitude permitted (i.e., 300 m/984 ft AFE for a twinjet), in an attempt to gain additional altitude and reduce the noise at the flyover noise measurement point (located at 6500 m/21,325 ft from brake release). Due to its larger thrust lapse and lower specific thrust relative to the CFM56-7B, a UHB engine throttle cutback is typically not as deep (in percent thrust), and a typical UHB-powered airplane does not climb as high over the flyover measurement point as the 737 reference model does. These thrust-lapse-related effects have an impact on flyover noise and their impact should be captured. Likewise, the UHB engine throttle setting on the 3-degree glide slope approach is typically higher than the CFM56-7B (in percent thrust). This also has an impact on the approach noise that should be taken into account. All of these trajectory-related effects on noise are captured in this analysis.

D. Exhaust Emissions

Oxides of nitrogen pose a health hazard to animal and plant life near sea level and are a potential ozone destruction risk in the stratosphere. In gas turbine engines, they are predominantly produced thermally via the Zeldovich chain reaction when ordinary nitrogen in the air comes into contact with high-temperature regions inside the combustor. There, nitrogen oxidizes into nitric oxide (NO), and much of it subsequently oxidizes further into nitrogen dioxide (NO₂), which are collectively known as NO_x. NO_x is one of the commercial jet engine exhaust emittants regulated by international standards.^{18, 19} A landing and takeoff (LTO) cycle is defined in these regulations that is intended to represent a single airplane operational cycle near airports. This cycle consists of four operational segments, each having a different throttle setting. The parameter regulated – LTO NO_x – is the amount of NO_x (in grams) per kilonewton of maximum takeoff rated sea level thrust over the four segments of the operational cycle. LTO NO_x is the emissions metric subject to optimization in this study.

Empirical correlation models are often used in conceptual design studies to predict an engine's NO_x emission index (EINO_x, defined as masses of NO_x emitted per thousand masses of fuel burned). EINO_x values are then used to make LTO NO_x certification predictions. In this study, a correlation model developed during NASA's Ultra-Efficient Engine Technology Project is used to predict EINO_x. As one might expect, the model is a strong function of combustor average reaction temperature, represented in the correlation by the fuel-air ratio. But significant increases in NO have also been observed to be a function of combustor entrance temperature²⁰ and, to a lesser extent, combustor entrance pressure.^{21, 22} The correlation is therefore also a function of combustor entrance total temperature and total pressure. Each of these properties are predicted by NPSS as noted above. Other constants in the correlation model are calibrated to represent next-generation combustor emissions technology levels and are fixed.

Most of the LTO NO_x is produced during the two cycle segments having the highest thrust settings, when the combustor reaction temperatures are highest. The combustor temperature during maximum takeoff rated conditions is fixed across the engine design space and is limited by hot section materials constraints, as noted above. Therefore the largest changes in LTO NO_x are brought about by changes in combustor entrance conditions. The Boolean design switch for OPR_{ADP} will be shown to have a large influence on LTO NO_x.

LTO NO_x is entirely independent of any airplane characteristic (indeed, in certification, it is measured on an engine test stand). It is linked in this study to airplane-related metrics (such as airplane ramp weight) only by way of our multi-objective system optimization.

E. Certification Noise

The certification noise analysis approach, assumptions, and tools used in this study have been examined by acoustics experts from NASA Glenn, NASA Langley, U.S. industry, and academia as part of a comprehensive, multi-fidelity, NASA acoustic tool benchmarking activity.²³ The Aircraft Noise Prediction Program (ANOPP, Release Level 27),^{24, 25} is a systems-level code used in this study to compute certification noise for the airplanes. The certification noise predictions of the reference 737 described in Ref. 23 serve as a validation of the methods and tools used in this vehicle study.

Freefield, lossless, 1/3rd octave band frequency component source noise levels are computed using predictive modules within ANOPP. The UHB engine's thermodynamic, aeromechanical, and geometry data are used as inputs to ANOPP's propulsion source noise prediction methods. At NASA, the NPSS and WATE airbreathing component element libraries have functions, viewers, and case files coded in interpretive language to produce engine data to be used as ANOPP input parameters. These so-called "engine state tables" are the preferred method to transfer engine

state data to ANOPP's source noise prediction modules. Engine state data – consisting of pressure, temperature, flow area, spool speed, and fuel and air flow rates – are computed by NPSS for a range of airspeeds, altitudes, and throttle settings at standard acoustic day (ISA+18°F) conditions. As the airplane traverses its flight path, engine data at the appropriate airspeed, altitude, atmospheric conditions, and throttle setting are interpolated from the state tables and are delivered to the source noise prediction modules.

The UHB engine's hardwall fan, jet, and core noise sources are predicted using ANOPP's Heidmann,²⁶ Stone,²⁷ and Emmerling^{28, 29} methods, respectively. Propulsion noise reduction technologies considered include nozzle chevrons, conventional double-degree-of-freedom fan acoustic liners, soft vane stators,³⁰ and over-the-rotor foam metal treatment.³¹ The latter two fan noise reduction technologies are anticipated to have matured enough for incorporation in the UHB engine assumed in this study. These technologies are also assumed to be relatively lightweight, inexpensive, low-maintenance, and free of aerodynamic performance penalties such that an engine manufacturer would be willing to make use of them on their product. In engine designs equipped with variable-area bypass nozzles, chevrons are assumed present for the central core nozzle only (chevrons are not applied to the bypass nozzle due to potential conflict with the actuation system needed for the nozzle design).

Freefield, lossless, 1/3rd octave band spectra for flap, slat, landing gear, and trailing edge airframe noise sources are predicted using a method developed by M.R. Fink for the FAA.³² The Fink method accepts gross airframe dimensions such as span, flap chord lengths, and gear configuration and dimensions. Recent scrutiny of portions of the Fink method has not yet revealed any fundamental issues.³³ The noise reduction technologies applied to the airframe are landing gear fairings, slat cove fillers, and flap porous tips. These technologies are considered mature enough to be available by our 2015 timeframe.³⁴

Descriptions of how each of these noise reduction technologies are used and their assumed acoustic benefits are described in detail in Refs. 1 and 4.

Using an assumption of acoustic superposition, the freefield, lossless spectra for all of the noise sources described above are analytically summed in the vicinity of the aircraft. Real noise sources are, of course, complex, distributed signals that are affected by other acoustic sources, aircraft external surfaces, and the environment. No provisions are made to adjust the component spectra for acoustic near-field phenomena such as source interactions, reflections, refraction, diffraction, or other effects.

The summed spectra are propagated to the three certification observers on the ground in accordance with the specifications for certification measurements. Noise propagation effects accounted for include spherical spreading, Doppler shift and convective amplification, atmospheric attenuation, ground reflections based on data for grass-covered ground, and extra ground attenuation. More complex propagation phenomena such as scattering, weather effects, and terrain are not modeled. The airplane trajectory, computed as described earlier, is fed into the ANOPP simulation. Vector geometry analyses for the airplane relative to the three certification microphone measurement locations are performed within ANOPP as functions of source time. The propagated acoustic spectra are predicted at half-second intervals at each of the three certification locations on the ground. From these propagated spectra, ANOPP computes several noise metrics of interest as functions of observer time. The Effective Perceived Noise Level (EPNL) certification noise metric is computed from the noise-time history at each observer as prescribed in Ref. 16.

In noise certification parlance, the cumulative, or algebraic, sum of the three certification EPNLs is often used to capture the range of operating conditions. The cumulative noise margin with respect to the Stage 4/Chapter 4 regulatory stringency is used for the overall noise metric in this paper.

F. Single- and Multi-Objective Optimization

Single-objective and multi-objective optimal solutions are sought, in various combinations, for block fuel burned, ramp weight, cumulative Stage 4 noise margin, and LTO NO_x emission objectives.

Single-objective optimal solutions are straightforward. They are obtained using one of the search-strategy optimizers built into the FLOPS code while parametrically varying the propulsion system design parameters externally in NPSS and WATE. The FLOPS optimizer used is the quasi-Newton Broyden-Fletcher-Goldfarb-Shanno method along with a Fiacco-McCormick penalty function strategy to account for constraints.

The multi-objective, Pareto-optimal solutions are handled differently. Pareto-optimal solutions are non-dominated sets where the value of one objective cannot be improved without punishing another. Classical methods of identifying Pareto-optimal solutions are commonly of the "preference" type. Preference methods usually begin by defining a single composite objective using the problem's multiple objective functions. The composite objective is optimized while parametrically altering the preferences for each of the underlying objectives until a Pareto solution is computed. The simplest example of a preference solution is the weighted sum method, where a single composite objective is formed by assigning weighting factors to, and adding together, each function in the objective space, with

the sum of the weighting factors equal to unity. A point-by-point, single-objective searching algorithm is then used to optimize the composite objective, while the weighting factors are varied, until the frontier is fully defined.

However, given the complexity of this problem, and with its combination of continuous-real and discontinuous Boolean design parameters in the decision space, a single-objective search-strategy optimizer may have difficulty in arriving at all of the optimal solutions along the frontier without excessive wandering or improperly centering over local optima. The Boolean design parameters also create a mathematically disconnected objective space that is somewhat difficult with which to work. In addition, unavoidable mathematical “noise” due to the convergence tolerances and the use of disparate tools that define the objective space (i.e., NPSS, FLOPS, ANOPP, etc.), may confound many single-objective search-strategy optimizers. This particular problem is also burdened by occasional “non-converged” points – most commonly in the engine aeromechanical analysis – where the optimizer is left to deal with no information returned from the analysis. It therefore may be difficult to use any classical, composite-objective, preference method for this problem. In addition, it will be shown that some regions of the objective space are mathematically nonconvex (i.e., regions surrounded by inflection points in the Pareto front), which classical multi-objective methods, at best, have difficulty defining.

For these reasons, an evolutionary multi-objective algorithm is chosen. The Non-dominated, Sorting Genetic Algorithm, NSGA-II,³⁵ is selected for its speed (relative to many other evolutionary optimizers) and its ability to control crowding and obtain solution diversity. NSGA-II uses a constrained tournament selection process consisting of crossover and mutation variation operators to define each generation. Binary crossovers involve simple exchanges of genes between parent members, while real-parameter crossovers use a Simulated Binary Crossover method.³⁶ Random changes are also introduced in each generation using real and binary mutation operators. The method’s no-penalty-parameter approach to constraint handling has been shown to achieve convergence while maintaining good population diversity.³⁷

The use of NSGA-II, or any evolutionary multi-objective algorithm, is not without its disadvantages. Although NSGA-II ranks among the fastest of evolutionary methods, it is still computationally expensive when compared to search-strategy methods; typically requiring about two weeks on a modest platform (an Intel® Core™ 2 Duo) to run the problems presented here to completion. Like search-strategy methods, NSGA-II may also be hampered by non-converged cases. In a non-converged case, large numerical values are assigned to each objective function, which has the effect of steering the optimizer away from that area of the design space. These occurrences have the potential to cause difficulties in the NSGA-II child selection process and to slow down the convergence to the Pareto-optimal solution.

III. Results and Discussion

The automated multidisciplinary analysis described above is applied to the following optimization problems. The objectives are, in various combinations, ramp weight, block fuel burned, cumulative Stage 4 noise margin, and LTO NO_x emissions.

A. Minimum Ramp Weight Solution (One Objective)

The solution for minimum ramp weight is an interesting, classical, single-objective aircraft optimization problem. Minimizing ramp weight is of particular interest because ramp weight is often used as a proxy for vehicle cost. Note that, in this context, ramp weight refers to the maximum permissible airplane takeoff gross weight “on the ramp” before takeoff. FLOPS determines ramp weight by iterating the design maximum gross weight (and the resulting structural weights, etc.) until the available fuel weight is sufficient to complete the specified design mission.

The problem is formally stated as follows. Mathematical nomenclature similar to that used in Ref. 35 is used. The single objective function, f_1 , Eq. (1), the independent continuous-real design parameters, x_1 through x_3 , Eqs. (2), the discontinuous-logical design parameters, x_4 through x_7 , Eqs. (3), and the inequality constraints, g_1 through g_7 , Eqs. (4), are written as

$$f_1 = \frac{W_{ramp} \text{ (lb)}}{150,000} \quad (1)$$

$$\begin{aligned} x_1 &= \frac{S_W \text{ (ft}^2\text{)}}{1400} & x_2 &= \frac{F_{N,SLs} \text{ (lb)}}{26,000} & x_3 &= FPR_{ADP} & (2) \\ 0.8 \leq x_1 &\leq 1.6 & 0.8 \leq x_2 &\leq 1.6 & 1.35 \leq x_3 &\leq 1.70 \end{aligned}$$

$$\begin{aligned}
 x_4 &= \text{Fan Drive System} & x_5 &= \text{OPR}_{ADP} & x_6 &= \text{Low spool PR Split} & x_7 &= \text{Variable Nozzle} & (3) \\
 x_4 &= \begin{cases} \text{Direct Drive} \\ \text{Gear Drive} \end{cases} & x_5 &= \begin{cases} \text{Low (32)} \\ \text{High (42)} \end{cases} & x_6 &= \begin{cases} \text{Low} \\ \text{High} \end{cases} & x_7 &= \begin{cases} \text{True} \\ \text{False} \end{cases}
 \end{aligned}$$

$$\begin{aligned}
 g_1(\bar{x}) &= 1 - \frac{D_{TO} \text{ (ft)}}{7000} \geq 0 & g_2(\bar{x}) &= 1 - \frac{D_L \text{ (ft)}}{7000} \geq 0 & g_3(\bar{x}) &= 1 - \frac{v_{app} \text{ (kt)}}{150} \geq 0 \\
 g_4(\bar{x}) &= \frac{\dot{h}_{pot,toc} \text{ (ft/min)}}{300} - 1 \geq 0 & g_5(\bar{x}) &= \frac{W_{excess \text{ fuel}} \text{ (lb)}}{10,000} \geq 0 & g_6(\bar{x}) &= \frac{F_{N,ss} \text{ (lb)}}{1000} \geq 0 & (4) \\
 g_7(\bar{x}) &= \frac{F_{N,mapp} \text{ (lb)}}{1000} \geq 0
 \end{aligned}$$

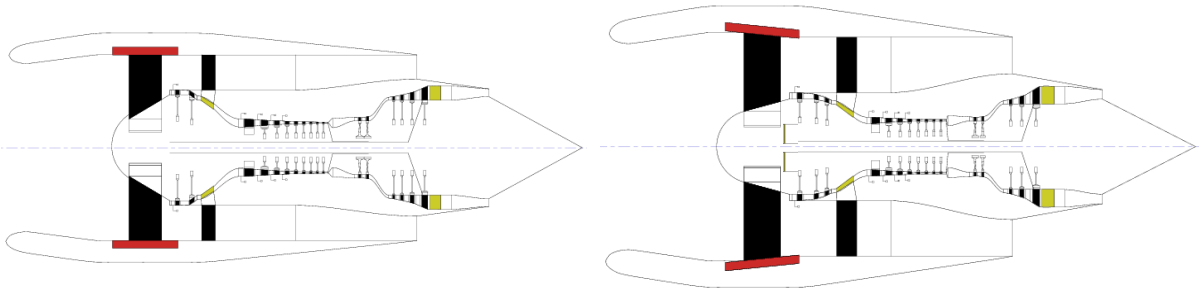


Figure 2. Turbofan for the minimum ramp weight airplane (left); turbofan for the airplane having the lowest block fuel while minimizing ramp weight (right).

Note that all parameters are made dimensionless and are normalized to equivalent orders of magnitude by dividing by appropriate constants. The design parameters x_1 and x_2 represent wing size and engine size and are the most important variable parameters in a classic airplane-engine sizing problem. x_3 through x_7 are the propulsion design parameters discussed in the previous section. The inequality constraints g_1 through g_7 represent typical airplane performance sizing requirements for field length, approach velocity, potential climb rate at top-of-climb (service ceiling) conditions, excess fuel weight (wing fuel capacity), and excess thrust for the second-segment climb and missed approach, respectively. Note that range is not one of the constraints as the ramp weight is sized to meet the required range independent of the optimization. All of the g_i must be non-negative for the solution to be feasible.

A single-objective optimum is easily found by conventional means and does not necessarily require the NSGA-II evolutionary optimizer. Indeed, it is often preferable to perform the optimization using a conventional search-strategy optimizer to more precisely locate the optimum, or to use graphical means to gain insight to the problem.

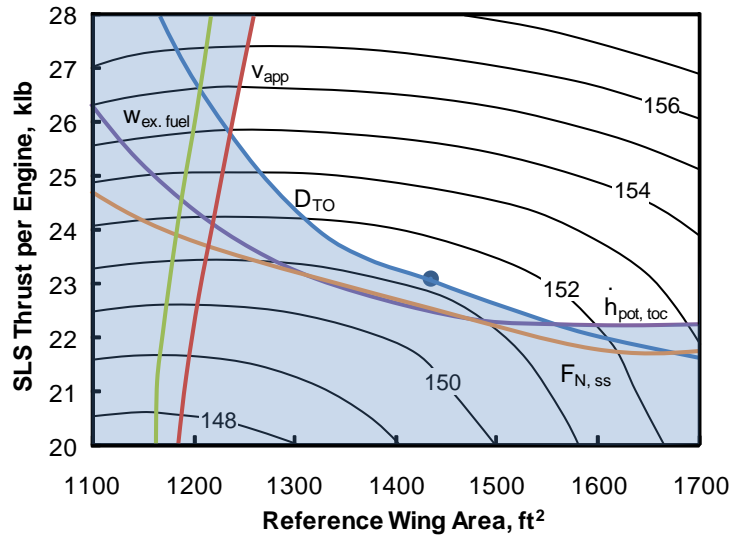


Figure 3. Sizing Diagram for the airplane having the lowest block fuel while minimizing ramp weight.

The analysis is performed by running a single-objective constrained optimization in x_1 and x_2 (that is, a classical wing and engine sizing) for permutations of x_3 through x_7 . Solutions are chosen by examination.

The propulsion system representing the minimum ramp weight solution (at 150,800 lbs) has a directly-driven fan, a “high” OPR, a “low” work split, and a fixed-geometry bypass nozzle. The ADP FPR is at the maximum value allowed (1.70) for a single-stage fan, which sets the bypass ratio at about 10. This engine is noted in Ref. 3 and is shown in Fig. 2 (left). The block fuel burned for this design is 31,250 lbs. And, although they are calculated outcomes rather than objectives, its Stage 4 cumulative noise margin and LTO NO_x emissions are -8.4 EPNdB and 25.6 g/kN, respectively.

However, with very little sacrifice in ramp weight, an interesting compromise solution exists that results in the lowest block fuel while minimizing ramp weight. Note this solution differs slightly from the *global* minimum for block fuel (a solution presented immediately below, where block fuel is cast as f_1 in a single-objective optimization). The compromise solution is discovered by running parametric sweeps in engine designs (i.e., varying x_3 through x_7) while minimizing ramp weight, and then simply choosing the design having the lowest block fuel. This propulsion system has a gear-driven fan, a “high” OPR, a “high” work split, a fixed-geometry bypass nozzle, and an ADP FPR of 1.48. The FPR is high enough that a variable-geometry bypass nozzle does not appear to be required and its extra weight is not justified. Here, the block fuel is at its lowest (30,400 lbs), while the ramp weight (151,200 lbs) is only 0.3% higher than the ramp weight global minimum. The Stage 4 cumulative noise margin and LTO NO_x emissions are -21.1 EPNdB, and 22.1 g/kN, respectively. This “compromise solution” engine, shown in Fig. 2 (right), is referred to in Ref. 3 as perhaps the best balanced engine design when all performance metrics are considered. A graphical sizing diagram for this solution is shown in Fig. 3. Ramp weight objective function contours are shown in black (in klb), and the design solution is shown by the circle. Five of the seven constraints (g_i) considered are also plotted, but takeoff field length is the only active (i.e., binding) constraint. Infeasible design space is shaded. When a single-objective search-strategy optimizer is used, the optimum point may be found precisely, even when it lies against a constraint.

B. Minimum Block Fuel Solution (One Objective)

The minimum block fuel weight solution is usually important in finding the minimum cash-direct operating cost design. It is also exactly the same as minimizing block CO_2 emissions. The single objective function, f_1 , is written as

$$f_1 = \frac{W_{\text{block fuel}} \text{ (lb)}}{30,000} \quad (5)$$

The independent design parameters, x_i , and the inequality constraints, g_i , are the same as Eqs. (2) through (4). The FLOPS optimizer is used as above, with block fuel as the single objective. The propulsion system representing the minimum block fuel solution (at 29,800 lbs) has a gear-driven fan, a “high” OPR, a “high” compression work split, and a variable-geometry bypass nozzle. The ADP FPR is 1.36: very nearly at the minimum value allowed (1.35). Ramp weight is 154,900 lbs; only 3% higher than the case for minimum ramp weight. The Stage 4 cumulative noise margin and LTO NO_x emissions are -27.8 EPNdB and 19.2 g/kN, respectively. The engine diagram is similar in overall architecture and turbomachinery stage counts to the engine shown in Fig. 2 (right) and is not shown here.

It is interesting to note the dramatic differences in engine design for the minimum ramp weight and minimum block fuel cases. The minimum ramp weight design prefers a conventional architecture, low-weight, compact, high FPR engine, while the minimum block fuel design prefers an alternative, gear-driven fan architecture with excellent fuel efficiency, a very low FPR, a high-diameter fan, and a variable-geometry bypass nozzle. This is perhaps to be expected, since a minimum-fuel airplane design should demand the most fuel-efficient engine possible, and would tolerate – to a degree – any reasonable penalties corresponding to such an engine (such as engine weight, diameter, landing gear weight, and nacelle drag penalties).

A FPR of only 1.36 leads to a rather large, 83-inch diameter fan. Very long main landing gear are required to provide adequate ground clearance for the engine nacelle. Although changes in gear length and weight are accounted for in this analysis, gear integration and internal wing packaging are not. A more detailed analysis would be required to determine if this engine design could really be accommodated in an underwing configuration.

Also worth noting is that, when considering ramp weight and block fuel objectives, it is always preferable to select the “high” OPR logical design switch. The higher OPR designs (42 at the ADP) have thermal efficiency benefits that are not offset by turbomachinery weight and length penalties.

C. Minimum Block Fuel and Noise Solution (Two Objectives)

The NSGA-II evolutionary algorithm is used for this two-objective problem. The population size is set at 48 members. The objectives are defined as

$$f_1 = \frac{W_{block\ fuel} \text{ (lb)}}{30,000} \quad f_2 = \frac{NM_{Cum} \text{ (EPNdB)}}{25} \quad (6)$$

f_2 is the Stage 4 cumulative certification noise margin (NM_{Cum}) normalized to the same order of magnitude as f_1 . The independent design parameters, x_i , and the inequality constraints, g_i , are the same as Eqs. (2) through (4).

The analysis was stopped after 167 generations (with over 8000 designs analyzed) when it became apparent that the solution was converging exclusively on low-FPR, geared engine designs. This should be expected, since the lowest noise designs and the lowest block fuel designs both occur at very low FPRs. Low-FPR, high-bypass-ratio engine cycles have very little jet noise. And, with our assumption of constant design fan loading, low-FPR cycle designs also have quite low, subsonic fan tip speeds and are thus free of rotor-shock-related fan noise sources. With propulsion noise reduction technologies being equal, the minimum noise solution naturally occurs at the lowest FPRs possible.

Therefore, the simultaneous solution of both objectives focuses on a narrow range of FPR between 1.35 (the minimum allowed) and 1.37. In other words, this is a case of virtually non-conflicting objectives, and only a very limited Pareto-optimal solution is possible. In mathematical terms, the cardinality of this Pareto-optimal set is approximately unity.

This is excellent news, since it is widely believed at NASA that meeting our aggressive noise and fuel burn goals simultaneously is not possible. It is for that reason that the NASA Subsonic Fixed Wing Project's goals are often called "corners of the design trade space," where one or two goals may be met simultaneously, but only at the expense of another. These results show that there is not a significant tradeoff between minimizing fuel and minimizing noise when selecting the cycle design characteristics of an engine. Meeting NASA's aggressive goals remains difficult, but low-FPR, geared, UHB turbofans appear to satisfy the requirements of minimizing fuel and minimizing noise.

The Pareto-optimal solution is shown graphically in Fig. 4. All feasible solutions are shown in the chart on the left. The dominated points are retained to illustrate how the optimizer considered, but discarded, direct-drive fan architectures (red triangles) in favor of geared fans (blue diamonds). No direct-drive engines survive the optimizer's selection process that, in this case, favors low-FPR designs. A detailed view of the small, non-dominated Pareto front is shown in the chart on the right. Note the change in scale. Propulsion systems with "high OPRs" are shown using open symbols, while systems with "low OPRs" are shown using closed symbols. All of these low-FPR engines along the frontier are geared. No differentiation between "low" or "high" compression work split designs is

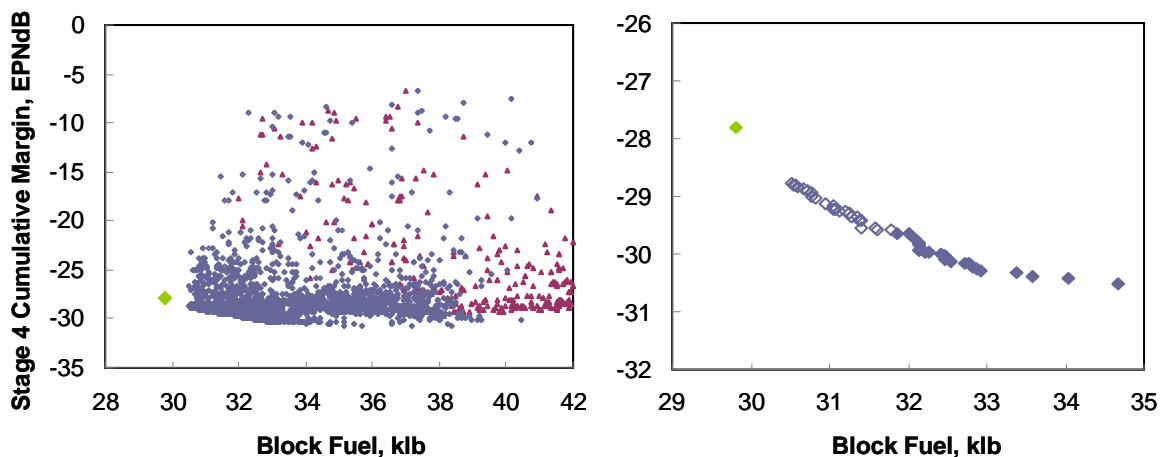


Figure 4. Pareto-optimal solutions for minimum block fuel and noise. *Left: all feasible solutions, showing geared engines (blue diamonds) and direct-drive engines (red triangles); Right: A detailed view of the small, non-dominated front, showing high-OPR engines (open symbols) and low-OPR engines (solid symbols). The global block fuel minimum is marked by the green diamond.*

noticeable after 167 generations, although eventually a preference for one or the other may be expected. The low-OPR engine designs are slightly quieter (the core noise model used is sensitive to compressor exit pressure and temperature), but being less thermally efficient, they consume more fuel. With the clustering in objective space around very low FPRs, the range in block fuel values along the small frontier is less than 1300 lbs for the high OPR designs.

Note that the minimum block fuel found here (30,500 lbs) is not as low as the single-objective minimum found in the Section B above (29,800 lbs; marked by the green symbol in both charts of Fig. 4). An examination of the lowest block fuel non-dominated frontier point revealed that it had not yet converged on optimum wing and engine sizes. Given enough generations, it is possible the minimum block fuel design of 29,800 lbs discovered in Section B would have been found here.

The global minimum solution for noise margin – although not determined directly by a single-objective optimization – appears to be approximately -30.5 EPNdB. It is achieved with a very low-FPR, low-OPR, geared fan design.

D. Minimum Ramp Weight and Noise Solution (Two Objectives)

A much broader Pareto front may be expected for this solution, since the FPR for the global minimum ramp weight (1.70) is far removed from the FPR preferred for minimum noise (1.35). The objectives for this problem are defined as

$$f_1 = \frac{W_{ramp} \text{ (lb)}}{150,000} \qquad f_2 = \frac{NM_{Cum} \text{ (EPNdB)}}{25} \qquad (7)$$

As before, the evolutionary algorithm is used with a population size of 48, and the independent design parameters, x_i , and the inequality constraints, g_i , are the same as Eqs. (2) through (4).

The analysis was interrupted after 198 generations with 9504 designs analyzed (2628 of them feasible). The Pareto-optimal solution is shown graphically in Fig. 5. Once again, all feasible solutions are shown in the chart on the left, while a more detailed view of the non-dominated Pareto front is shown on the right. Note the change in scale.

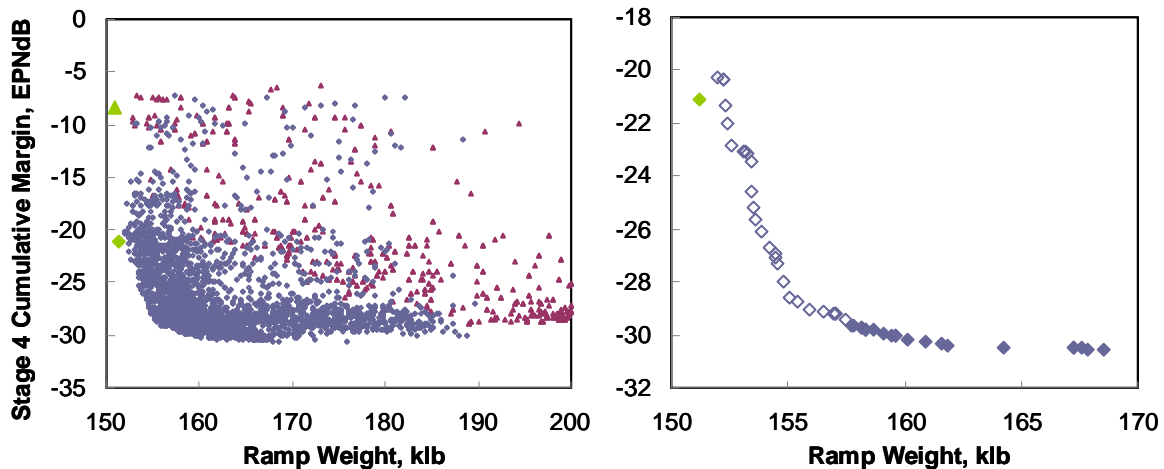


Figure 5. Pareto-optimal solutions for minimum ramp weight and noise. *Left: all feasible solutions, showing geared engines (blue diamonds) and direct-drive engines (red triangles); Right: A detailed view of the non-dominated front, showing high-OPR engines (open symbols) and low-OPR engines (solid symbols). The global ramp weight minimum is marked by the green triangle; the “best compromise” design is marked by the green diamond.*

Once again, the global minimum solution for noise margin appears to be approximately -30.5 EPNdB with an engine design similar to that found above in Section C. The minimum ramp weight of 152,000 lbs shown in the Pareto front is achieved with a gear-driven fan system with a FPR of 1.48. This is somewhat unexpected, since, in Section B, the global minimum ramp weight is deterministically found via single-objective optimization to be a direct-drive fan design at 150,800 lbs (marked by the green triangle in Fig. 5). Several competitive direct-drive

engine designs (marked by the red triangles) can be seen in Fig. 5 near 153,000 lbs, but they are all dominated by geared engine designs (at least after 198 generations). It is possible that, given sufficient time, the minimum ramp weight, direct-drive design of 150,800 lbs discovered in Section B would have been found.

As it is, however, this evolutionary optimization comes remarkably close to the best “compromise solution” engine design described in Section B (its ramp weight is 151,200 lbs; marked by the green diamond in Fig. 5). That design, found deterministically via single-objective optimization, also has a nearly-identical, gear-driven fan design with a FPR of 1.48.

Note the low-noise designs in Fig. 5 with ramp weights heavier than 190,000 lbs. These are solutions having direct-drive engines with very low FPRs. Although they are feasible solutions, the engines are, of course, very long and heavy, with many LPT stages. The evolutionary optimizer likely discovered these solutions using its crowded comparison operator feature while attempting to extend the frontier towards lower-noise designs. In general, however, most unreasonable engine designs are effectively avoided by the optimizer.

This two-objective optimization clearly shows the trade between ramp weight and noise. Given constant technology levels, improvements in one objective cannot be made without punishing the other. This illustrates the difficulty in designing extremely quiet aircraft, such as those called for by NASA’s Subsonic Fixed Wing goals. While it perhaps can be done, it is often uneconomical to do so.

E. Minimum Ramp Weight and NO_x Solution (Two Objectives)

Cycles with higher ADP FPRs have higher OPRs at SLS conditions due to engine specific thrust and thrust lapse characteristics, even if the OPRs at the ADP are designed to be identical. At SLS conditions (where the LTO NO_x metrics are measured), cycles having higher ADP FPRs have higher combustor entrance temperatures and pressures and therefore have higher levels of LTO NO_x. Thus, a Pareto front would be expected in a multi-objective optimal solution of ramp weight and LTO NO_x.

This behavior is in contrast to the optimal solution of block fuel and LTO NO_x, where minima for both of those objectives would tend to cluster around low-FPR engine designs. Since a case of non-conflicting objectives has already been shown (i.e., the minimum block fuel and noise solution in Section C), a minimum block fuel and LTO NO_x problem is not presented here.

Once again, we note that LTO NO_x is an engine-only metric and is entirely independent of any airplane characteristic. It is linked here to ramp weight only by way of our multi-objective system optimization.

The objectives for the minimum ramp weight and LTO NO_x problem are defined as

$$f_1 = \frac{W_{ramp} \text{ (lb)}}{150,000} \qquad f_2 = \frac{LTO \text{ NO}_x \text{ (g/kN)}}{20} \qquad (8)$$

The same method, design parameters, and constraint vector as before are used. The analysis was interrupted after 143 generations with 6864 designs analyzed (2773 of them feasible). The Pareto-optimal solution is shown graphically in Fig. 6. All feasible designs are shown, with the dependency of fan drive system shown on the left, and the dependency of the OPR setting shown on the right.

Once again, the optimizer did not have enough time to discover the global minimum ramp weight represented by a high-FPR, high-OPR, direct-drive engine design (marked by the green triangle in the figure), but it did come very close to the compromise design represented by a geared fan design (marked by the green diamond). The lower boundaries of the objective space are horizontal and flat because the optimizer found the NO_x minimum at the limiting 1.35 FPR boundary. As it is, the minimum LTO NO_x solution is nearly identical to the minimum noise margin solution found in the previous two sections.

There are noticeable regimes marked by high-OPR (aqua diamonds) and low-OPR (coral triangles) engine cycles. For combustors of equivalent emissions technology and effectiveness, low-OPR cycles should result in lower LTO NO_x. There is noticeable symmetry between the low- and high-OPR regimes. That is, one regime has the same general shape as the other, and they are offset in the objective space by the same amounts. Of course, this is an artifact of OPR being represented as a logical design parameter; if OPR were a continuous-real parameter, two regimes would not be visible and the frontier would not be nonconvex. In any case, the distinct regime behavior permits a generalization: if an engine is designed with a “high” OPR of 42, it should produce approximately 15% higher LTO NO_x and have a 1.5% lower ramp weight than one designed with a “low” OPR of 32, if the engines are otherwise similarly designed. An alternate, and perhaps more appropriate, way to interpret the data is that the high-OPR “best compromise” design (the green diamond) has 36% higher NO_x than the lightest, low-OPR, low-NO_x design (158 klb, 16.2 g/kN).

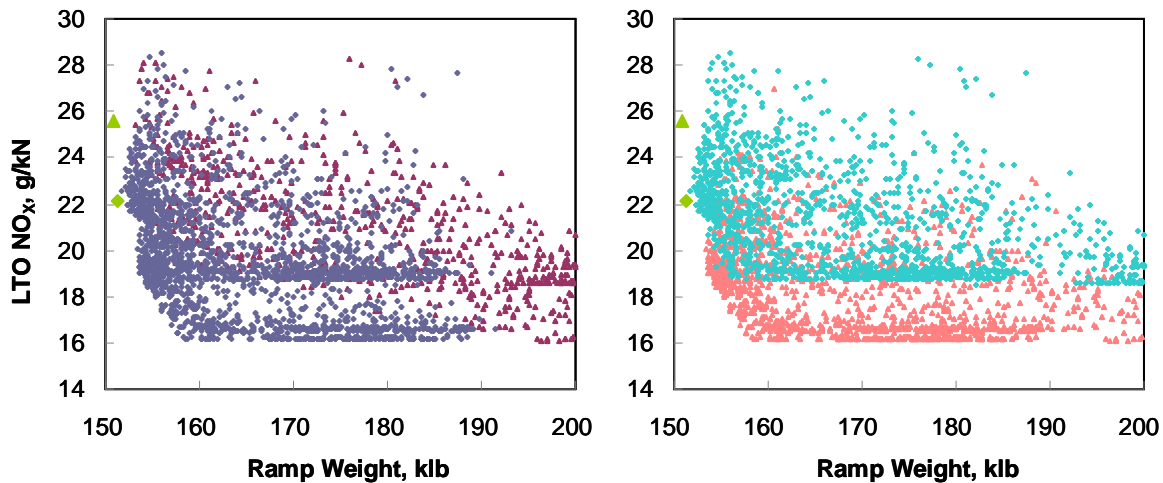


Figure 6. Pareto-optimal solutions for minimum ramp weight and LTO NO_x. *Left: all feasible solutions, showing geared engines (blue diamonds) and direct-drive engines (red triangles); Right: all feasible solutions, showing high-OPR engines (aqua diamonds) and low-OPR engines (coral triangles). The global ramp weight minimum is marked by the green triangle; the “best compromise” design is marked by the green diamond.*

F. Engine Design Considerations

The chief objective in engine design is minimum airplane life cycle cost, while achieving acceptable levels of operational safety, risk, and environmental impact. Vehicle cost is indirectly addressed in this study by predicting its classical surrogate indicator: ramp weight. The block fuel weights predicted are important in finding the minimum cash-direct operating cost design. Safety and risk are much more complex to assess, but they are indirectly recognized here by selecting only technologies mature enough for consideration.

Every attempt has been made in this analysis to provide an unbiased, independent, accurate assessment of aircraft powered by UHB turbofans. Thermodynamic cycle and aeromechanical engine design methods, and even the analytical tools used (NPSS, for example, is a U.S. industry standard) follow engineering state-of-the-practice.

However, the caveat must be stated that *the optimal engine designs described here have been found for our analytical model, and not necessarily for the true problem.* The engine design approach and technology assumptions used for this study are not exclusive. There are a number of possible variations in the design approach; such as different choices for the ADP (particularly the cruise Mach number), thrust sizing conditions, different cooling philosophies, or a different choice of extraction ratio. Furthermore, our assumptions of future technology levels are speculative. Changes in the technology assumptions and design approach can affect the absolute engine performance and weight, as well as the relative differences among the engine types. All of this together makes our analytical model potentially inexact. The results of this study should be viewed, therefore, in light of the assumptions and approach used. With that reader caution stated, the following engine design recommendations are made.

Higher engine OPR and the resulting thermal efficiency benefits always appear justified for ramp weight and block fuel metrics, despite increases in turbomachinery weight, engine length, and cooling air temperature. The maximum OPR (42) is set in this study by a reasonable compressor exit annular duct height constraint. However, LTO NO_x emissions are higher for high-OPR engine designs (for given combustor technology levels) due to higher combustor entrance temperature and pressure. There is also a slight increase in core noise for high-OPR engine designs. In advanced UHB engines, core noise may become significant – even at higher throttle settings – since jet and fan noise are lower due to increased bypass ratio, low fan tip speeds, and modern, more effective noise reduction technologies. Accurate core noise modeling for UHB engines is essential. A need is foreseen for improved engine core noise modeling methods at NASA that reflect the high overall pressure ratios of modern engines.

At sufficiently low values of FPR, turbofan engine cycles require some type of variable geometry to avoid fan surge margin problems near sea level and to ensure proper operation throughout the flight envelope. Although it is not the only option, the variable-geometry bypass nozzle appears to be a practical means to enable low-FPR, UHB turbofans.

A summary of each of the optimum solutions discussed in Sections A through E is presented in Table 1.

Table 1. Summary of optimum solutions.

Description	FPR	Fan Drive	OPR	W_{ramp} (lb)	$W_{\text{block fuel}}$ (lb)	NM_{Cum} (EPNdB)	LTO NO_x (g/kN)
Min. Ramp Wt.	1.70	Direct	42	150,800	31,250	-8.4	25.6
Min. Block Fuel	1.36	Geared	42	154,900	29,800	-27.8	19.2
Ramp Wt. and Fuel Compromise	1.48	Geared	42	151,200	30,400	-21.1	22.1
Min. Noise	1.35	Geared	32	169,000	34,650	-30.5	16.5
Min. LTO NO_x	1.35	Geared	32	158,300	31,800	-30.3	16.2

One of the most important design options considered in this study is the fan drive system. This study is not intended to be an endorsement – or an indictment – of either gear-driven or directly-driven fan designs. Arguments for both engine architectures are given below.

1. The Case for Gear-Driven Fans

The benefits of fuel efficiency that accompany geared turbfans are very attractive. A fan gearbox effectively solves the classical low-spool shaft speed mismatch problem corresponding to low-FPR engine designs. With low FPRs made possible by a geared drive, more enthalpy is available from the LPT that may be used to increase the bypass ratio to ultrahigh levels. A gearbox is thus an enabling technology to dramatic gains in propulsive efficiency.

A gearbox also provides greater freedom in designing the low-pressure compressor, particularly for engines with low-pressure compressors shouldering a greater portion of the overall pressure ratio. Since it rotates rapidly, the low-pressure compressor may have a high pressure ratio with a practical number of stages.

Furthermore, a gearbox appears to justify its additional weight when FPR is sufficiently low. With a gearbox, the LPT need not have a great number of stages when the FPR becomes small. And the fuel efficiency benefits that are inherent in low-FPR, high-bypass-ratio engine cycles pay off dramatically in reduced fuel weight. The best compromise engine design and the minimum block fuel engine design described in Parts A and B of this section, respectively, are geared engines.

Engines having very low FPRs – geared, typically – are also very quiet, since the bypass ratio increases as FPR decreases. If the bypass ratio is high enough, jet noise becomes a minor contributor to community noise (see Ref. 4). Fan noise is also greatly reduced, particularly if the FPR is low enough to justify subsonic fan tip speeds at takeoff and all shock-related fan noise sources vanish. And as we have seen in Part E of this section, low-FPR engine cycles can also be low in LTO NO_x emissions (for combustors of equivalent emissions technology and effectiveness).

The gearbox extends the range of viable FPRs to lower levels and effectively widens the engine cycle design space. If engine size and integration issues can be overcome, geared turbfans have the potential to extend the bypass ratio into the UHB range.

2. The Case for Directly-Driven Fans

Despite the apparent advantages of geared turbfans, direct-drive turbfans remain a good design choice. Direct-drive turbfans result in the lowest engine weight, vehicle ramp weight, and operating empty weight, and, by inference, the lowest vehicle cost.

Engines having higher FPRs – directly-driven, typically – can have relatively small, compact nacelles with less wetted area and drag than higher-diameter geared engines. They also simplify landing gear design. Although the effects of landing gear length and weight are accounted for in this study, the impacts of gear integration, retraction, and internal wing packaging are not. Likewise, the aerodynamic effects of high-diameter engines are accounted for here, but only to the first-order. A higher-fidelity modeling of high-diameter geared engine issues is called for, such as nacelle-wing interference drag effects and engine-out drag and its impact on tail sizing. Moreover, no gearbox maintenance is necessary for direct-drive turbfans.

Furthermore, a large portion of the direct-drive turbfan design space remains unexplored in this study. Constant design fan loading is assumed here – that is, as FPR is reduced, fan tip speed is reduced as well. The classical low-spool shaft speed mismatch problems associated with lower-FPR, direct-drive engines can be alleviated somewhat by using lightly-loaded fans. More fuel-efficient, direct-drive engines having moderately lower FPRs and higher

bypass ratios may have been discovered in this assessment if fan loading was treated as a design parameter. Also, and perhaps counterintuitively, lower burner temperatures may lead to better direct-drive engines. Lowering the gas temperature lowers the speed of sound in the hot section, and can mitigate the shaft speed mismatch by effectively increasing the LPT tip Mach numbers. Turbine cooling and hot section material benefits may exist as well. Attractive, lower-temperature, direct-drive engine designs with lightly-loaded fans may exist throughout the design space.

IV. Conclusions

Single- and multi-objective optimized solutions are presented for the multidisciplinary design of ultrahigh bypass ratio engines applied to an advanced, notional, single-aisle airplane. NASA's Subsonic Fixed Wing Project goals serve as optimization objectives. This study is intended to provide independent information to NASA program management to help guide its technology development efforts.

Identifying a "best" engine design depends entirely on the metric(s) of interest. The engine design for minimum ramp weight – a traditional aircraft optimization objective – is found to be a high-FPR, high-OPR, direct-drive turbofan. Although its turbomachinery, material selection, cooling, and construction technologies are assumed to be advanced, it may yet be said to be of a conventional architecture. Block fuel, however, is minimized by a strikingly different engine design: a low-FPR, high-OPR, geared UHB turbofan with a variable-geometry bypass nozzle. And between these two extremes, an excellent "compromise" engine design exists – a moderate-FPR, high-OPR, geared turbofan – that nicely balances the ramp weight and block fuel metrics. This engine also has relatively low community noise and NO_x emissions.

An interesting finding is how, when multiple objectives are considered, some metrics may be improved upon simultaneously. It is widely believed at NASA that meeting our aggressive noise and fuel burn goals simultaneously is not possible. However, block fuel and noise appear to be minimized together by selecting similar engine cycle design characteristics (i.e., low-FPR, geared, UHB turbofans). NO_x exhaust emissions are minimized by low-FPR, geared designs as well, although NO_x is minimized more dramatically by lowering OPR. Other metrics, when taken together as multiple objectives, form classical Pareto frontiers, where one metric cannot be improved without punishing another. Optimization has the potential to discover many engine designs that acceptably satisfy multiple objectives.

Ultimately the primary metric is life cycle cost, while achieving acceptable levels of environmental impact and achieving operational safety. Historically, ramp weight has been used as a surrogate indicator for life cycle cost in aircraft design and optimization. However, recent increases in fuel cost have made fuel consumption a more important factor in the calculation of life cycle cost. It may no longer be valid to assume the lowest ramp weight configuration has the lowest life cycle cost.

Acknowledgments

We would like to thank the other members of the NASA Intercenter Systems Analysis Team who worked on the initial ultrahigh bypass ratio engine study that preceded this analysis. William Haller, Douglas Thurman, Kenneth Fisher, and Michael Tong, your work is appreciated. We would also like to thank the Subsonic Fixed Wing Project of NASA's Fundamental Aeronautics Program for supporting this effort.

References

¹Guynn, M.D., Berton, J.J., Fisher, K.L., Haller, W.J., Tong, M.T., and Thurman, D.R.: "Engine Concept Study for an Advanced Single-Aisle Transport," NASA TM-2009-215784, August, 2009.

²Guynn, M.D., Berton, J.J., Fisher, K.L., Haller, W.J., Tong, M.T., and Thurman, D.R.: "Analysis of Turbofan Design Options for an Advanced Single-Aisle Transport Aircraft," 9th AIAA Aviation Technology, Integration, and Operations (ATIO) Conference, September, 2009.

³Guynn, M.D., Berton, J.J., Fisher, K.L., Haller, W.J., Tong, M.T., and Thurman, D.R.: "Refined Exploration of Turbofan Design Options for an Advanced Single-Aisle Transport," NASA TM to be published, 2010.

⁴Berton, J.; Envia, E.; and Burley, C.: "An Analytical Assessment of NASA's N+1 Subsonic Fixed Wing Project Noise Goal," AIAA Paper 2009-3144, 15th AIAA/CEAS Aeroacoustics Conference (30th AIAA Aeroacoustics Conference), Miami, FL, 11-13 May, 2009.

⁵Norris, G.; and Wall, R.: "Boeing Goes Back to Drawing Board for 737 Follow-on," *Aviation Week and Space Technology*, 18 May, 2008.

⁶Polek, G.: "Boeing, Airbus Commit to Re-engining Decisions by Year-end," *Aviation International News*, 26 February, 2010.

- ⁷Claus, R.W.; Evans, A.L.; Lytle, J.K., and Nichols, L.D.: "Numerical Propulsion System Simulation," *Computing Systems in Engineering*, Vol. 2, No. 4, pp. 357-364, 1991.
- ⁸NPSS User Guide Software Release: NPSS_1.6.5.
- ⁹Onat, E., and Klees, G.: "A Method to Estimate Weight and Dimensions of Large and Small Gas Turbine Engines," NASA CR 159481, 1979.
- ¹⁰McCullers, L.A.: "Aircraft Configuration Optimization Including Optimized Flight Profiles," *Proceedings of the Symposium on Recent Experiences in Multidisciplinary Analysis and Optimization*, NASA CP 2327, April 1984.
- ¹¹Ardema, M.D., Chambers, M.C., Patron, A.P., Hahn, A.S., Miura, H., and Moore, M.D., "Analytical Fuselage and Wing Weight Estimation of Transport Aircraft," NASA TM-110392, May 1996.
- ¹²*Jane's Aero-Engines*, Jane's Information Group, Alexandria, VA (various).
- ¹³787 Dreamliner Program Fact Sheet, URL: <http://www.boeing.com/commercial/787family/programfacts.html> [cited 6/8/2010].
- ¹⁴Gloudemans, J.R.; Davis, P.C.; and Gelhausen, P.A.: "A Rapid Geometry Modeler for Conceptual Aircraft," AIAA-1996-0052, January, 1996.
- ¹⁵U.S. Code of Federal Regulations, Title 14, Chapter I, Part 25. *Airworthiness Standards: Transport Category Airplanes*.
- ¹⁶U.S. Code of Federal Regulations, Title 14, Chapter I, Part 36. *Noise standards: Aircraft type and airworthiness certification*.
- ¹⁷"737 Airplane Characteristics for Airport Planning," D6-58325-6, Boeing Commercial Airplanes, October 2005.
- ¹⁸*International Standards and Recommended Practices – Environmental Protection, Annex 16 to the Convention on International Civil Aviation, Volume II: Aircraft Engine Emissions*, 2nd Edition, International Civil Aviation Organization (ICAO), Montreal, Canada, July 1993.
- ¹⁹U.S. Code of Federal Regulations, Title 14, Chapter I, Part 34. *Fuel Venting and Exhaust Emission Requirements for Turbine Engine-Powered Airplanes*.
- ²⁰Rink, K.K.; and Lefebvre, A.H.: "The Influence of Fuel Composition and Spray Characteristics on Nitric Oxide Formation," *Combustion, Science and Technology*, vol. 68, pp. 1-14, 1989.
- ²¹Correa, S.M.: "Lean Premixed Combustion for Gas Turbines: Review and Required Research," *Fossil Fuel Combustion*, ASME PD-Vol. 33, 1991.
- ²²Leonard, G.L.; and Correa, S.M.: "NO_x Formation in Lean Premixed High-Pressure Methane Flames," *Second ASME Fossil Fuel Combustion Symposium*, PD-30, pp. 69-74, 1990.
- ²³Dahl, M.D. (ed.): "Assessment of NASA's Aircraft Noise Prediction Capability," NASA TP-20XX-215653, to be published.
- ²⁴Gillian, R.E.: "Aircraft Noise Prediction Program User's Manual," NASA TM-84486, 1983.
- ²⁵Zorumski, W.E.: "Aircraft Noise Prediction Program Theoretical Manual," NASA TM-83199, 1981, Parts 1 and 2 (Currently maintained at NASA Langley Research Center by the ANOPP team in electronic format and provided upon request; Latest revision: January 2009).
- ²⁶Kontos, K.B.; Janardan, B.; and Gliebe, P.R.: "Improved NASA-ANOPP Noise Prediction Computer Code for Advanced Subsonic Propulsion Systems Volume 1: ANOPP Evaluation and Fan Noise Model Improvement," NASA CR-195480, 1996.
- ²⁷Stone, J.R., Krejsa, E.A., Clark, B.J., and Berton, J.J.: "Jet Noise Modeling for Suppressed and Unsuppressed Aircraft in Simulated Flight," NASA TM-2009-215524, 2009.
- ²⁸Emmerling, J.J.; Kazin, S.B.; and Matta, R.K.: "Core Engine Noise Control Program. Volume III, Supplement 1 - Prediction Methods," FAA-RD-74-125, III-I, Mar. 1976 (Available from DTIC as AD A030 376.)
- ²⁹Ho, P.Y.; and Doyle, V.L.: "Combustion noise prediction update," 5th AIAA Aeroacoustics Conference, Seattle, WA, AIAA Paper 1979-0588, 1979.
- ³⁰Jones, M.; Parrott, T.; Sutliff, D.; Hughes, C.: "Assessment of Soft Vane and Metal Foam Engine Noise Reduction Concepts," 15th AIAA/CEAS Aeroacoustics Conference, AIAA-2009-3142, 2009.
- ³¹Sutliff, D.L.; Jones, M.G.; and Hartley, T.C.: "Attenuation of FJ44 Turbofan Engine Noise with a Foam-Metal Liner Installed Over-the-Rotor," 15th AIAA/CEAS Aeroacoustics Conference (30th AIAA Aeroacoustics Conference), Miami, FL, AIAA Paper 2009-3141, 2009.
- ³²Fink, M.R.: "Airframe Noise Prediction Method," FAA-RD-77-29, March, 1977.
- ³³Humphries, W.M.; Burley, C.L.; and Brooks, T.F.: "Scale-Model Landing Gear Noise Spectra and Directivity," Acoustics Technical Working Group Meeting, 23-24 Sep. 2008, Williamsburg, VA, United States.
- ³⁴Envia, Edmane: "Progress Toward N+1 Noise Goal," Fundamental Aeronautics Program, Subsonic Fixed Wing Project, 12-Month Program Review, Washington, DC, November 5-6, 2008.
- ³⁵Deb, K.; Pratap, A.; Agarwal, S.; and Meyarivan, T.: "A Fast and Elitist Multi-Objective Genetic Algorithm: NSGA-II," *IEEE Transactions on Evolutionary Computation*, vol. 6, no. 2, pp. 181-197, 2002.
- ³⁶Deb, K.; and Agrawal, R. B.: "Simulated Binary Crossover for Continuous Search Space," *Complex Systems*, vol. 9, no. 2, pp. 115-148, 1995.
- ³⁷Deb, K.; Pratap, A.; and Meyarivan, T.: "Constrained Test Problems for Multi-objective Evolutionary Optimization," *Proceedings of the First International Conference on Evolutionary Multi-Criterion Optimization*, Zurich, Switzerland, pp. 284-298, March 7-9, 2001.